PAPER

Evaluating metal–organic frameworks for post-combustion carbon dioxide capture *via* temperature swing adsorption†

Jarad A. Mason,[a] Kenji Sumida,[a] Zoey R. Herm,[a] Rajamani Krishna*[b] and Jeffrey. R. Long*[a]

Two representative metal–organic frameworks, $Zn_4O(BTB)_2$ (BTB^{3-} = 1,3,5-benzenetribenzoate; MOF-177) and $Mg_2(dobdc)$ ($dobdc^{4-}$ = 1,4-dioxido-2,5-benzenedicarboxylate; Mg-MOF-74, CPO-27-Mg), are evaluated in detail for their potential use in post-combustion CO_2 capture *via* temperature swing adsorption (TSA). Low-pressure single-component CO_2 and N_2 adsorption isotherms were measured every 10 °C from 20 to 200 °C, allowing the performance of each material to be analyzed precisely. In order to gain a more complete understanding of the separation phenomena and the thermodynamics of CO_2 adsorption, the isotherms were analyzed using a variety of methods. With regard to the isosteric heat of CO_2 adsorption, $Mg_2(dobdc)$ exhibits an abrupt drop at loadings approaching the saturation of the Mg^{2+} sites, which has significant implications for regeneration in different industrial applications. The CO_2/N_2 selectivities were calculated using ideal adsorbed solution theory (IAST) for MOF-177, $Mg_2(dobdc)$, and zeolite NaX, and working capacities were estimated using a simplified TSA model. Significantly, MOF-177 fails to exhibit a positive working capacity even at regeneration temperatures as high as 200 °C, while $Mg_2(dobdc)$ reaches a working capacity of 17.6 wt % at this temperature. Breakthrough simulations were also performed for the three materials, demonstrating the superior performance of $Mg_2(dobdc)$ over MOF-177 and zeolite NaX. These results show that the presence of strong CO_2 adsorption sites is essential for a metal–organic framework to be of utility in post-combustion CO_2 capture *via* a TSA process, and present a methodology for the evaluation of new metal–organic frameworks *via* analysis of single-component gas adsorption isotherms.

[a]*Department of Chemistry, University of California, Berkeley and Materials Sciences Division, Lawrence Berkeley National Laboratory, Berkeley, CA, 94720, USA. E-mail: jrlong@berkeley.edu*
[b]*Van't Hoff Institute for Molecular Sciences, University of Amsterdam, Science Park 904, 1098 XH Amsterdam, The Netherlands. E-mail: r.krishna@uva.nl*

† Electronic supplementary information (ESI) available: Complete experimental characterization, heat capacity measurements under He, measured adsorption isotherm data, details of the single-site and dual-site Langmuir fits, methodology for calculating isosteric heats of adsorption from a dual-site Langmuir model, methodology for conversion of adsorption excess loadings to absolute loadings, and video animations obtained from the adsorber model simulations for CO_2/N_2 breakthrough on $Mg_2(dobdc)$ and zeolite NaX. See DOI: 10.1039/c1ee01720a

Introduction

As concerns over the environmental impact of rising carbon dioxide emissions from anthropogenic sources continue to mount, it is becoming increasingly evident that the world's energy demands must be met in a more sustainable way.[1] With regard to fuel combustion, coal-fired power plants contribute more than 40% to annual global CO_2 emissions, and this number is projected to increase over the next several decades as a result of economic growth and increased industrialization in developing nations.[2] Although a shift in the global infrastructure toward cleaner energy sources is crucial for the reduction of greenhouse

---

Broader context

The development of an effective carbon dioxide capture system is critical to reducing global greenhouse gas emissions and moving toward a cleaner energy future. Metal-organic frameworks are particularly promising as CO_2 capture materials, because their high surface areas and adjustable pore functionality enables the selective adsorption of large quantities of CO_2. The primary cost in any CO_2 capture process is the energy required to regenerate the adsorbent after it has become saturated with CO_2. In metal-organic frameworks, the strength of the interaction of CO_2 with the pore surface can be tuned to minimize the energy required for capturing a given amount of CO_2. Here, we present a detailed study of how two representative frameworks can be expected to behave in a real CO_2 capture process. The methodology employs just easily measurable single-component gas adsorption isotherms at relevant flue gas pressures and regeneration temperatures, and provides a general means for comparing the efficacies of different solid adsorbents.

gas emissions, such a transition is expected to proceed gradually owing to the need to modify or replace major components of the existing energy framework. Consequently, efforts to mitigate the rising levels of CO_2 in the short-term *via* the development of effective methods for CO_2 capture and sequestration are of high priority.[3]

One potential scenario under which CO_2 capture could be rapidly deployed is in the context of post-combustion capture and storage, wherein the CO_2 is selectively removed from a power plant flue gas stream and sequestered through storage in underground geological formations.[4] In existing capture technologies employing aqueous alkanolamine solutions (amine "scrubbers"), the primary cost of the capture process is associated with the high energy requirements needed for regeneration of the capture media.[5] Indeed, as much as 40% of the energy output of the power plant is required to evolve the CO_2 from the solutions, with much of the energy being expended in heating the water itself to the regeneration temperature.[6] Thus, materials that feature a lower energy penalty for regeneration, while maintaining a high selectivity towards CO_2 over the other components of the flue gas, are crucial for improving the efficiency of CO_2 capture.

Metal–organic frameworks present a promising platform for the development of next-generation capture materials as a result of their high capacity for gas adsorption and tunable pore surfaces that can facilitate highly selective binding of CO_2.[7,8] Note that the composition of a typical flue gas dictates the separation to be primarily a CO_2/N_2 separation, although the presence of other lesser components, such as H_2O, O_2, CO, SO_x, and NO_x, must also be considered when assessing the performance of new materials. Nevertheless, the high degree of control over the surface functionalities within the pores of metal–organic frameworks is expected to enable the precise tuning of the optimal affinity towards CO_2, allowing the total energy penalty of the CO_2 capture process to be reduced to levels approaching the predicted minimum of 11%.[9a]

The regeneration of an industrial solid adsorbent is usually accomplished *via* pressure swing adsorption (PSA), vacuum swing adsorption (VSA), temperature swing adsorption (TSA), or a combination of these processes.[10] Since each of these regeneration methods implies a different set of ideal adsorbent properties, this actually presents the possibility of tailoring the industrial regeneration process to match the properties of a given metal–organic framework. However, among these methods, TSA is particularly promising for post-combustion CO_2 capture, owing to difficulties with compressing or applying a vacuum to such large volumes of a low-pressure gas stream, as well as to the potential availability of low-grade heat in a power plant as a source of energy for regeneration.[9] Thus, the energy requirement for CO_2 capture utilizing TSA may be significantly reduced over the corresponding PSA or VSA processes. As illustrated in Fig. 1, a TSA cycle involves heating the saturated adsorbent under ambient pressure to desorb the captured gas and regenerate the capture material.

Despite the promise of metal–organic frameworks for use in a post-combustion CO_2 capture scenario, their performance within a TSA-based capture process has not yet been examined in detail. Indeed, despite the large body of literature investigating CO_2 adsorption within this class of materials, the range of
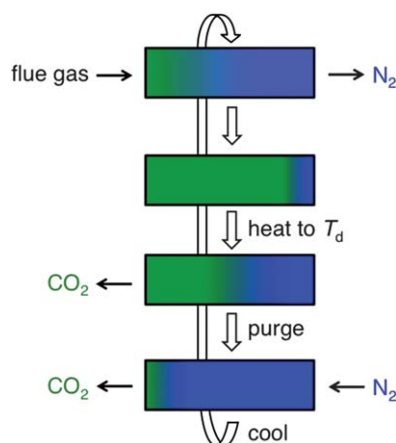

Fig. 1 Schematic diagram of an idealized temperature swing adsorption (TSA) process for post-combustion CO_2 capture.[12] Flue gas is introduced to the fixed bed, which selectively adsorbs CO_2 (green) over N_2 (blue) until the bed is saturated with CO_2. The flue gas is then redirected, and the bed is heated to the desorption temperature, T_d. The CO_2 is desorbed from the bed and then pushed out by an N_2 purge until the CO_2 rich stream coming off the bed falls below a desired purity level. The bed is then cooled and readied for the next adsorption cycle.

temperatures for which adsorption isotherms have been reported is significantly narrower than the scope of temperatures that may be reasonably considered for a TSA-based process. Indeed, to the best of our knowledge, the highest temperature CO_2 isotherms at the relevant pressures (< 1 bar) reported for metal–organic frameworks are around 70 °C,[11] which is still far lower than the likely range of 100–200 °C to be employed as the desorption temperature within an actual TSA CO_2 capture system.[12] Thus, in order to more fully understand the performance and properties of metal–organic frameworks in this type of process, there is an urgent need for low-pressure CO_2 adsorption experiments to be performed at higher temperatures.

Herein, we report the first detailed study of metal–organic frameworks in a temperature swing setting, and provide a methodology for assessing the likely performance of new materials within a real TSA system. For such an application, metal–organic frameworks fall into two general categories of potential interest: those with an exceptionally high specific surface area presenting only weak physisorptive sites, such as present in an activated carbon, and those that in addition feature strong adsorption sites designed specifically for binding CO_2. With a BET surface area of 4690 m²/g and a high capacity for CO_2 at high pressure, $Zn_4O(BTB)_2$ (BTB^{3-} = 1,3,5-benzenetribenzoate; MOF-177) was selected as representative of the former class of materials.[7d,13] In contrast, $Mg_2(dobdc)$ ($dobdc^{4-}$ = 1,4-dioxido-2,5-benzenedicarboxylate; Mg-MOF-74, CPO-27-Mg)[14b] possesses a somewhat lower BET surface area of 1800 m²/g, but features a high density of exposed Mg^{2+} cation sites following activation. The presence of these strong adsorption sites has been demonstrated to afford a significant CO_2 uptake at low pressures, leading to a high selectivity at the pressures relevant for CO_2 capture from a flue gas.[8b,14] Note that, beyond unsaturated metal coordination sites[15] of the type found in $Mg_2(dobdc)$, strong CO_2 binding sites can also be achieved through the use of polar functional groups[16] or

This journal is © The Royal Society of Chemistry 2011

Energy Environ. Sci., 2011, **4**, 3030–3040 | **3031**

functionalities inserted post-synthetically.[17] Importantly, the methodology we present provides a means of assessing the viability of any such material for TSA-based CO_2 capture through the analysis of simple single-component gas adsorption isotherms.

Experimental

General information

Anhydrous dichloromethane was obtained from a Vac anhydrous solvent system. All other reagents were obtained from commercial vendors and used without further purification. UHP-grade (99.999% purity) carbon dioxide, nitrogen, and helium were used for all adsorption measurements. Powder X-ray diffraction patterns were collected on a Bruker D8 Advance diffractometer with a Cu anode ($\lambda = 1.5406$ Å). Infrared spectra were obtained on a Perkin-Elmer Spectrum 100 Optica FTIR spectrometer furnished with an attenuated total reflectance accessory.

Synthesis and activation of MOF-177

The compound MOF-177 was synthesized as previously reported,[18] and was activated using a strategy adopted from a literature procedure.[19] The reaction product was transferred into a nitrogen-filled glove bag, where the solid was soaked in anhydrous DMF (50 mL) for 24 h. The supernatant was decanted and replenished twice over two days. The solid was then soaked in anhydrous dichloromethane (50 mL) for 6 h. The supernatant was decanted and replenished four times over three days. The product was stored in a glovebox under a dinitrogen atmosphere before activation under dynamic vacuum for 24 h. The successful synthesis and activation of the framework was confirmed by comparing the X-ray powder diffraction pattern, infrared spectrum, and Langmuir and BET surface areas to those previously reported (see Fig. S1 and S3†).

Synthesis and activation of Mg₂(dobdc)

The compound Mg_2(dobdc) was synthesized and activated using a strategy adopted from previous reports.[14b,c] Following the reaction of $Mg(NO_3)_2 \cdot 6H_2O$ and 2,5-dihydroxyterephthalic acid, the resulting yellow microcrystalline material was combined, washed repeatedly with N,N-dimethylformamide (DMF), and then soaked in DMF in a nitrogen-filled glove bag. After 24 h, the DMF was decanted, and freshly distilled methanol was added. The solid was then transferred to a nitrogen-filled glovebox. The methanol was decanted, and the solid was soaked in DMF on a hot-plate set at 100 °C for 18 h. The DMF was decanted and replaced, and the solid was soaked at 100 °C for 4 h. The DMF was decanted and replaced by methanol at room temperature, which was decanted and replenished six times with a minimum of 6 h between washes. The dark yellow powder was isolated and heated under dynamic vacuum at 180 °C for 24 h. The successful synthesis and activation of the framework was confirmed by comparing the X-ray powder diffraction pattern, infrared spectrum, and Langmuir and BET surface areas to those previously reported (see Fig. S2–S3 in the Supporting Information†).

Low-pressure gas sorption measurements and surface area calculations

Gas adsorption isotherms for pressures in the range 0–1.1 bar were measured using a Micromeritics ASAP 2020 instrument. Samples of MOF-177 and Mg_2(dobdc) were transferred under a dinitrogen atmosphere to preweighed analysis tubes, which were capped with a Transeal. The samples were evacuated on the ASAP until the outgas rate was less than 2 mTorr/min. The evacuated analysis tubes containing degassed samples were then carefully transferred to an electronic balance and weighed to determine the mass of sample (174 mg for MOF-177 and 91.5 mg for Mg_2(dobdc)). The tube was transferred back to the analysis port of the gas adsorption instrument. The outgas rate was again confirmed to be less than 2 mTorr/min. Langmuir and BET[20] surface areas were determined by measuring N_2 adsorption isotherms in a 77 K liquid nitrogen bath and calculated using the Micromeritics software. Adsorption isotherms between 20 and 80 °C were measured using a recirculating dewar (Micromeritics) connected to a Julabo F32-MC isothermal bath. In order to collect isotherm data above 80 °C, a thermocouple was affixed to the analysis tube using copper wire and connected to a Glas-Col DigiTroll II temperature controller. A furnace was connected to the temperature controller, placed around the analysis tube, and filled with sand. The temperature controller was set to the desired temperature, and the automatic tuning function was used to set the proportional-integral-derivative (PID) parameters and equilibrate the sand bath temperature. The error in sample temperature associated with each measurement using the furnace is estimated at ±0.3 °C. After each isotherm measurement, the sample was evacuated under dynamic vacuum, until the outgas rate was less than 2 mTorr/min, prior to continuing on to the next measurement.

High-pressure gas sorption measurements

In a typical measurement, at least 200 mg of sample was loaded in a sample holder in a glovebox under a dinitrogen atmosphere. Carbon dioxide excess adsorption measurements were performed on an automated Sieverts' apparatus (PCTPro-2000 from Hy-Energy Scientific Instruments LLC) over a pressure range of 0–50 bar. Pore volumes determined from the high-pressure data were 1.59 cm³/g for MOF-177 and 0.5727 cm³/g for Mg_2(dobdc). The absolute adsorbate loadings were obtained using the following procedure. The fluid densities at any given temperature were first determined using the Peng-Robinson equation of state. Subsequently, these values were multiplied by the pore volume of each material to obtain the loadings in the "bulk" of the pore space. Addition of the loadings in the "bulk" to the experimentally determined "excess" loadings yields the "absolute" component loadings. All isotherm fits, and subsequent analyses to determine selectivities and isosteric heats of adsorption, were carried out using the absolute loadings.

Heat capacity measurements

All thermal analyses were performed on a TA Instruments Q200 differential scanning calorimeter (DSC) equipped with a refrigerated cooling system RSC90 under a nitrogen or helium flow. Baseline data for the empty heating chamber was collected

between temperatures of −90 °C and 400 °C, followed by a temperature calibration using the melting point of an indium sample (m.p. 156.60 °C). The energy axis was calibrated by collecting heat flow data on a sapphire sample (21.8 mg) and fitting this data to the literature values.[21]

A sample of activated MOF-177 (6.5 mg) or $Mg_2(dobdc)$ (9.4 mg) was hermetically sealed within an aluminum pan in a glovebox under a nitrogen atmosphere, and the sample was quickly transferred to the calorimeter. The heat flow data were collected using a temperature ramp rate of 3 °C/min in the temperature range of −50 to 250 °C, using a temperature modulation of ± 1 °C every 60 s. The sample was then cooled back to −50 °C, the heating cycle was repeated a further two times, and the data for the three runs were averaged. The heat capacity was obtained using the following expression:

$$C_p(\text{sample}) = \frac{H_{\text{sample}}}{H_{\text{ref}}} \cdot \frac{m_{\text{ref}}}{m_{\text{sample}}} \cdot C_p(\text{ref}) \qquad (1)$$

where $C_p(\text{sample})$ and $C_p(\text{ref})$ represent the heat capacities of the sample and reference material (sapphire), H_{sample} and H_{ref} represent the heat flows for the sample and reference material detected by the calorimeter with respect to an empty aluminum pan, and m_{sample} and m_{ref} represent the experimental masses of the sample and reference material, respectively.

Results and discussion

Adsorption isotherm data

The low-pressure CO_2 and N_2 adsorption isotherms collected every 10 °C from 20 to 200 °C for MOF-177 and $Mg_2(dobdc)$ are presented in Fig. 2. As expected, the quantity adsorbed decreases with temperature for both gases as a result of the greater thermal energy of the molecules at higher temperatures. Additionally, the quantity of CO_2 adsorbed is higher than that for N_2 at all temperatures for both compounds as a result of the greater quadrupole moment and polarizability of CO_2 (13.4×10^{-40} C m² and 26.3×10^{-25} cm³, respectively) compared to N_2 (4.7×10^{-40} C m² and 17.7×10^{-25} cm³, respectively).[22] In the case of $Mg_2(dobdc)$, an initial steep increase in CO_2 uptake at low pressure is observed due to the presence of coordinatively-unsaturated Mg^{2+} sites on the surface of the material (see Fig. 2c).[14b] Such a behavior is characteristic of any material with high-affinity binding sites for CO_2. Importantly, as the temperature is increased, the initial steep rise in the data becomes less prominent, and the isotherms become nearly linear beyond 120 °C. This is presumably due to the thermal energy of the gas molecules overcoming the heat of adsorption at the exposed Mg^{2+} sites, resulting in an apparently homogenous surface at higher temperatures. In contrast, the lack of high-affinity binding
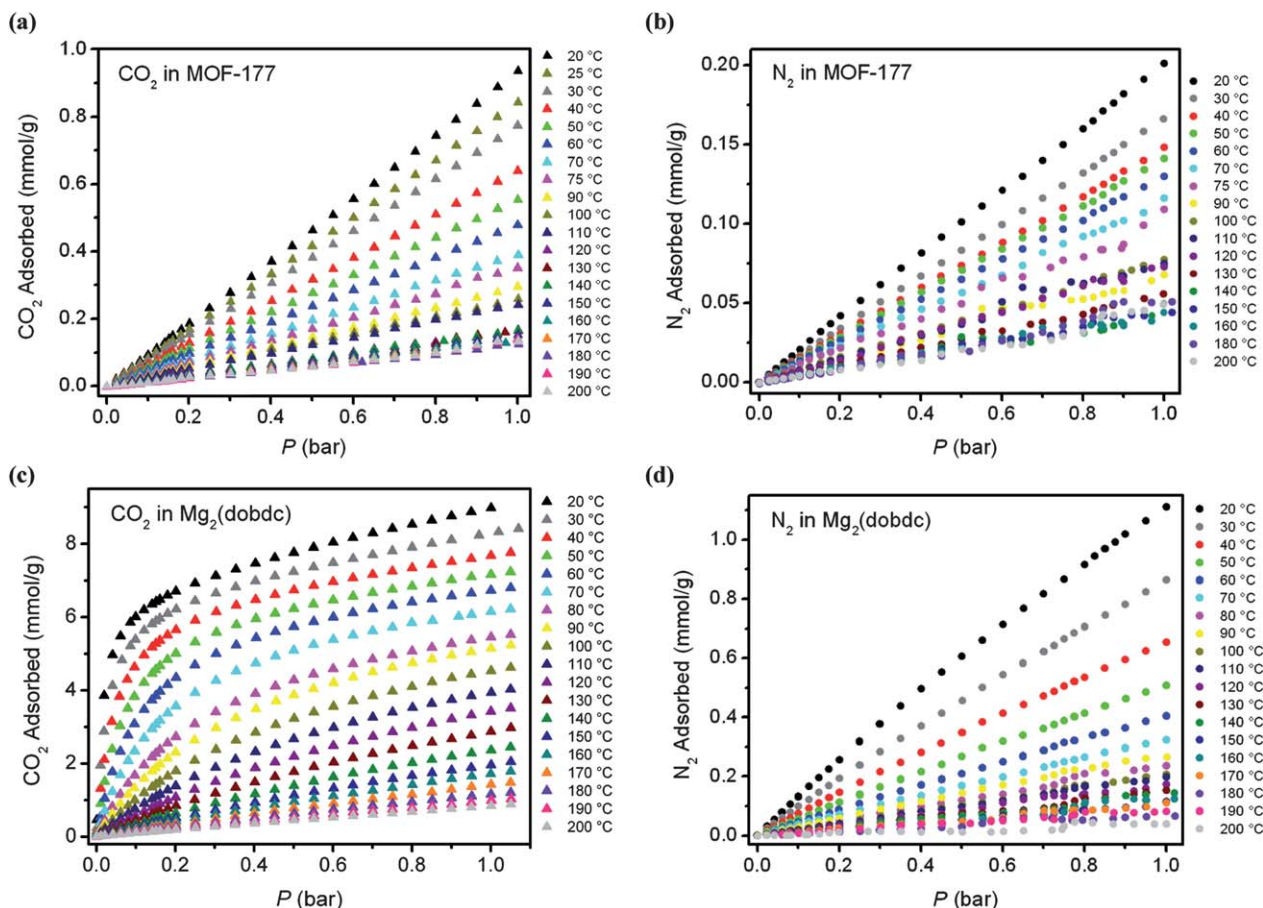

Fig. 2 Excess CO_2 (triangles) and N_2 (circles) adsorption isotherms for MOF-177 (a and b) and $Mg_2(dobdc)$ (c and d) measured from 20 to 200 °C.

sites within MOF-177 leads to a linear CO_2 adsorption isotherm across all temperatures, similar to what is commonly observed for activated carbons.

Post-combustion flue gas is released at a temperature in the range of 40 to 60 °C and at a total pressure of approximately 1 bar, wherein CO_2 is present at a relatively low partial pressure of 0.13–0.16 bar.[23] Thus, the adsorption capacity for CO_2 in the low-pressure region is critically important. Indeed, at 40 °C and 0.15 bar, Mg_2(dobdc) adsorbs 5.28 mmol/g CO_2 (18.9 wt %), while the corresponding adsorption capacity for MOF-177 is just 0.097 mmol/g CO_2 (0.43 wt %).[24] In post-combustion CO_2 capture, the solid adsorbent will likely be packed into a large fixed bed, and, as such, the volumetric uptake is also a vital consideration from the perspective of minimizing the size of the column towers, which may affect the heating efficiency during the regeneration step. In terms of the volumetric capacity, the high gravimetric uptake coupled with the relatively dense structure of Mg_2(dobdc) combine to provide a CO_2 uptake of 4.83 mmol/cm³ (213 g/L), while the large pores within MOF-177 lead to a volumetric capacity of just 0.041 mmol/cm³ (1.8 g/L).

The process design of a TSA system for any material requires precise knowledge of the thermodynamics of the adsorption of both CO_2 and N_2. Here, the single-component gas adsorption isotherms have been fit to allow the determination of precise isosteric heats of adsorption and to enable application of ideal adsorbed solution theory (IAST) in simulating the performance of each material under a mixed component gas. Although the N_2 adsorption isotherms for both MOF-177 and Mg_2(dobdc) and the CO_2 adsorption isotherms for MOF-177 can all be modeled adequately using a single-site Langmuir model, the simultaneous fitting of all the CO_2 isotherm data for Mg_2(dobdc) necessitates the use of a dual-site Langmuir model due to the inherent heterogeneity of the pore surface and the much higher affinity of CO_2 for the exposed Mg^{2+} cation sites compared to other adsorption sites within the material. The resulting fit of the adsorption isotherm data for Mg_2(dobdc) at 40 and 50 °C using
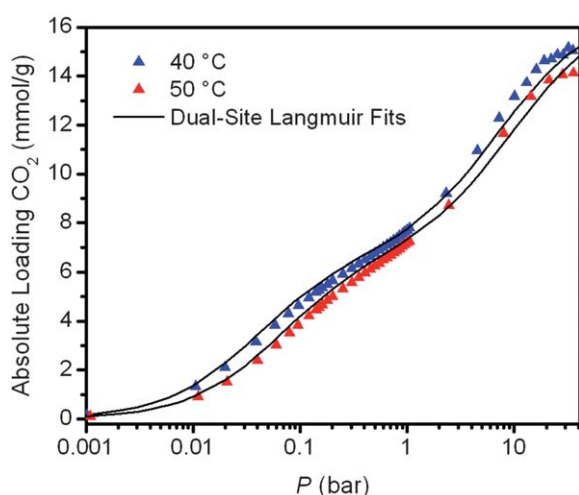

Fig. 3 Low- and high-pressure CO_2 adsorption isotherms for Mg_2(dobdc) at 40 and 50 °C, along with the corresponding dual-site Langmuir fits (black lines). Loadings have been converted from excess adsorption to absolute adsorption. Note that the fits shown result from simultaneously modeling all of the isotherm data collected between 20 and 200 °C, not just the data at 40 and 50 °C.

the dual-site Langmuir model is shown in Fig. 3 (see Fig. S11† for illustrations of the accuracy of the fit at other temperatures). Note that a single-site Langmuir isotherm cannot adequately describe the inflection that occurs for temperatures below 120 °C at loadings corresponding to roughly one CO_2 per Mg^{2+} center (calculated to be 8.24 mmol/g).[25] Hence, this simpler model is not able to fit the adsorption data at pressures below 1 bar, which is the region of interest for post-combustion CO_2 capture.

Although Mg_2(dobdc) represents an unusual case, in that it has an exceptionally high density of binding sites with a strong affinity for CO_2 in addition to a comparable number of relatively weak binding sites, similar arguments should hold for other metal–organic frameworks featuring a combination of strong and weak binding sites. Specifically, modeling of the lower-pressure adsorption isotherms using a single-site Langmuir model considering only the Mg^{2+} cation sites (and neglecting the weaker adsorption sites) is not appropriate even at low loadings due to the high-affinity sites becoming close to saturated at pressures well below 1 bar. It is expected that even below the ratio of 1 CO_2:Mg^{2+} site, there will be a distribution of occupied binding sites across all temperatures, resulting in the dual-site Langmuir model being necessary even at the lowest temperatures and pressures. This demonstrates the importance of selecting the most appropriate adsorption model, depending on the material and adsorbed gas, such that the isotherms can be consistently modeled across the entire pressure and temperature range.

Isosteric heat of adsorption

The regeneration temperature of a CO_2 capture material in a TSA process largely depends on the thermodynamics of adsorption. This is commonly expressed as the isosteric heat of adsorption, Q_{st}, which represents the average binding energy of an adsorbing gas molecule at a specific surface coverage. Isosteric heats of adsorption are often calculated by fitting isotherms at two or three different temperatures with the virial equation. In this work, however, we have instead fit the entire set of isotherms for all temperatures using the simplest physically-realistic single-site or dual-site Langmuir model.

Based on the single-site Langmuir fit, MOF-177 has a constant isosteric heat of adsorption of 14 kJ/mol (see Fig. 4), indicative of the relatively weak CO_2-adsorbent interaction observed in the CO_2 isotherms and lack of strong adsorption sites in the framework. Note that in contrast to a single-site Langmuir model, determination of the isosteric heat of adsorption from isotherms modeled using a dual-site Langmuir is complicated by the need to obtain an explicit analytical expression for pressure as a function of the loading for calculating Q_{st} (eqn (2)).

$$Q_{st} = RT^2 \left(\frac{\partial \ln p}{\partial T} \right)_q \qquad (2)$$

We have therefore developed an exact analytic procedure for calculating Q_{st} as a function of loading (see Supporting Information† for details). To the best of our knowledge, this represents the first time that isosteric heats of adsorption have been calculated from a dual-site Langmuir fit.

As a direct result of the inflection in the isotherm for CO_2 adsorption in Mg_2(dobdc), there is a corresponding inflection in the isosteric heat of adsorption curve, coinciding with the
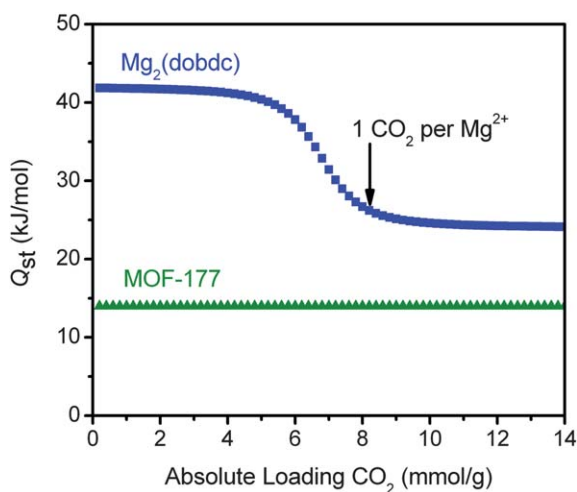
Fig. 4 Isosteric heat of adsorption, Q_{st}, as a function of absolute loading of CO_2 for MOF-177 and $Mg_2(dobdc)$ calculated at 40 °C using a single site Langmuir and dual-site Langmuir model, respectively. Note that Q_{st} is only weakly dependent upon temperature (see Fig. S12†).

saturation of the exposed Mg^{2+} adsorption sites (see Fig. 4). The isosteric heat of adsorption falls from 42 kJ/mol (corresponding approximately to the heat of adsorption for the strong sites) at loadings below 5 mmol/g to 24 kJ/mol (approximately the heat of adsorption for the weak sites) at loadings above 8 mmol/g. This is in excellent agreement with the calculated loading of 8.24 mmol/g corresponding to one CO_2 molecule per Mg^{2+} cation. Note that the zero-coverage isosteric heat of adsorption is also in good agreement with literature values, which were computed using conventional methods.[14b,d] However, previous reports have found an increase in Q_{st} at high loadings, which was attributed to increasing CO_2-CO_2 interactions.[8f,14d] In contrast, we were able to determine Q_{st} as a function of loading by fitting all of the CO_2 isotherms for $Mg_2(dobdc)$ simultaneously, using the large amount of low-pressure data from 20 to 200 °C and the corresponding high-pressure isotherms (see Fig. S12†), without needing to invoke CO_2-CO_2 interactions. It is important to note that absolute loadings, which are not experimentally measurable, must be used in the isotherm fits and subsequent determination of Q_{st}.[26] Failure to use absolute loadings will result in significant differences at high pressures, estimated to be as much as 10–12%, and likely gives rise to the increasing heats of adsorption at high loadings that have been reported previously. Additionally, Q_{st} is only a weak function of temperature, and the isosteric heat of adsorption curves do not change significantly at different temperatures.

For post-combustion CO_2 capture, the CO_2 is adsorbed at a partial pressure of 0.15 bar, and the resulting uptake of CO_2 is below 5.5 mmol/g at relevant flue gas temperatures (40–60 °C). Thus, the corresponding Q_{st} value is around 42 kJ/mol. Additionally, the sharp decrease in isosteric heat of adsorption is an important result that has direct consequences for the application of $Mg_2(dobdc)$, or any similar material, in other applications involving CO_2 capture. For instance, $Mg_2(dobdc)$ was recently studied for use as an adsorbent in hydrogen purification and in precombustion CO_2 capture.[27] Both of these applications require separation of CO_2 from H_2 at high pressures, and although

$Mg_2(dobdc)$ shows great promise with a high CO_2/H_2 selectivity and high working capacity, concerns were raised over the energy that would be required to regenerate the framework after CO_2 adsorption. The isosteric heat of adsorption calculations demonstrate, however, that the regeneration penalty is not as high as originally anticipated, since at 40 °C and 1 bar, $Mg_2(dobdc)$ has a CO_2 uptake of 7.7 mmol/g, with a relevant Q_{st} value around 24 kJ/mol. Consequently, for a PSA process operating between 1 and 40 bar, the regeneration energy should be significantly less than was originally expected for a 42 kJ/mol heat of adsorption, since most of the stronger binding sites will not need to be regenerated.

Selectivity

We now address the issue of determining the selectivity factor, S_{ads}, for binary mixtures using pure component isotherm data. The use of an adsorption model, such as IAST,[28] is essential in practice, because collection of experimental data for a mixed component gas cannot be conveniently and rapidly performed.[29] The accuracy of the IAST procedure has already been established for adsorption of a wide variety of gas mixtures in different zeolites[30] and for CO_2 capture within metal–organic frameworks.[31] The method is employed here for estimation of the adsorption selectivity across the entire temperature range for which single-component isotherms were collected for MOF-177 and $Mg_2(dobdc)$.

The IAST estimations of adsorption selectivities for CO_2 over N_2 were calculated for an idealized flue gas mixture composed of 0.15 bar CO_2 and 0.75 bar N_2 based on the fits to the isotherm data for MOF-177 and $Mg_2(dobdc)$ (see Fig. 5a). As one of the most studied adsorbents for CO_2 separation processes, the selectivities for zeolite NaX were also calculated from previously reported data for comparison.[32] Notably, MOF-177 has a selectivity factor near unity under these conditions, while $Mg_2(dobdc)$ demonstrates a tremendous selectivity, with an IAST selectivity factor of 148.1 at the typical flue gas temperature of 50 °C. Indeed, $Mg_2(dobdc)$ outperforms zeolite NaX, which has an IAST selectivity factor of 87.4 at 50 °C.

Gas adsorption selectivities for metal–organic frameworks are often reported simply as the ratio of number of moles of each component adsorbed at the relevant partial pressures in the individual single-component isotherms. Fig. 5a demonstrates the importance of using IAST to calculate selectivity values, especially when high-energy binding sites are present. For $Mg_2(dobdc)$, using the simpler selectivity calculation (eqn (3) with loadings, q_i, determined only from the single-component isotherms) not only produces very different values, but, significantly, the trend in selectivity as a function of temperature is inconsistent with the more physically accurate IAST model. With its greater polarizability and larger quadrupole moment,[22] CO_2 has stronger interactions with the open metal sites of $Mg_2(dobdc)$ than does N_2.[14b,e] As the thermal energy of the gas molecules increases, the difference in binding energies of CO_2 and N_2, which are reasonably constant with temperature, becomes less significant, and the selectivity should consequently decrease. This result demonstrates that IAST calculations are necessary in order to obtain reasonable selectivity values. It is also important to note that it is not generally appropriate to use the ratio of
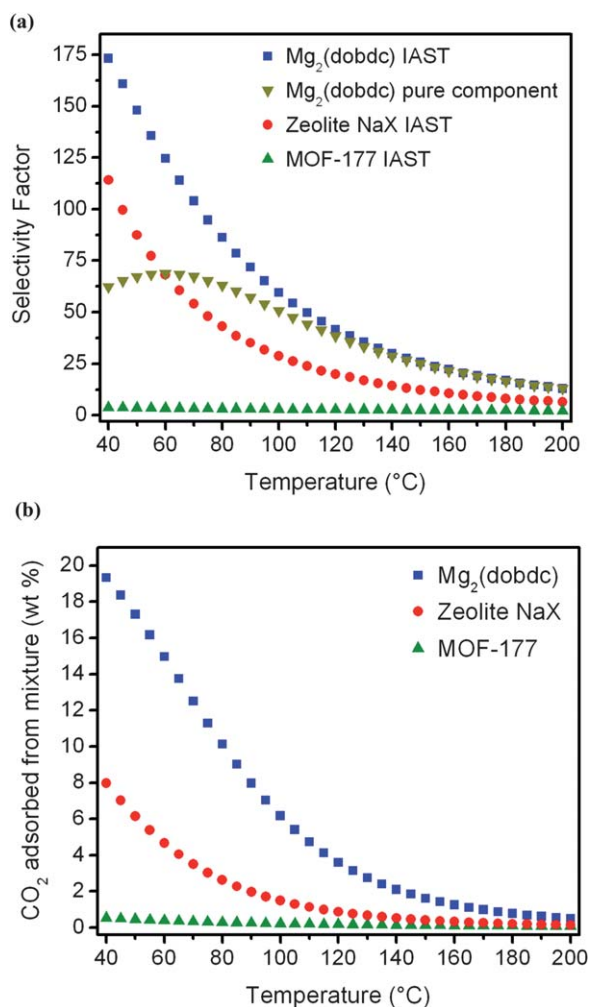
Fig. 5 (a) Selectivity factors as a function of temperature calculated using IAST for MOF-177, $Mg_2(dobdc)$, and zeolite NaX compared to the selectivity factors calculated from the pure component isotherms for $Mg_2(dobdc)$. (b) IAST calculations of weight percent of CO_2 adsorbed from a mixture of 0.15 bar CO_2 and 0.75 bar N_2 as a function of temperature for MOF-177, $Mg_2(dobdc)$, and zeolite NaX.

Henry's constants from each pure component isotherm as a means of calculating selectivities for post-combustion CO_2/N_2 separation, since, for example, the CO_2 uptake in $Mg_2(dobdc)$ is not in the linear Henry regime at the relevant flue gas conditions of 40 to 60 °C and 0.15 bar.

When evaluating any material for a particular application, it is important to determine selectivity factors at conditions relevant to that application. For post-combustion CO_2 capture, selectivity factors should be calculated for a mixture of approximately 0.15 bar CO_2 and 0.75 bar N_2, at around 50 °C.[23] For example, MOF-177 has a reasonably high CO_2/N_2 selectivity at 1 bar CO_2 and 1 bar N_2; however, this does not make MOF-177 a good candidate for any practical CO_2/N_2 separation due to its poor selectivity at the relevant partial pressures. In addition, it is important to clearly define how reported selectivity factors were calculated in order to facilitate the comparison of different materials. Selectivity factors should also be normalized to the

composition of the gas mixture as shown in eqn (3), where q_i is the uptake and p_i is the partial pressure of component i.

$$S_{ads} = \frac{q_1/q_2}{p_1/p_2} \tag{3}$$

Breakthrough simulations

A TSA process consists of adsorption and desorption cycles that rely on the raising and lowering of the system temperature. In this section, we focus on evaluating the separation performance of a material with a real mixed gas under the adsorption phase of a TSA process. In post-combustion CO_2 capture, the flue gas will likely pass through packed beds containing the solid adsorbent. Breakthrough measurements can provide a good indication of the performance of a material in such a system, but are challenging to perform accurately. Variations in particle size, column packing, and flow rates can lead to difficulties in comparing breakthrough measurement results for different samples. Breakthrough simulations therefore offer a convenient alternative. These were performed for MOF-177, $Mg_2(dobdc)$, and zeolite NaX in the temperature range 40–80 °C using a previously developed adsorber model—which incorporates IAST to describe local thermodynamic equilibrium between the gas phase that is in contact with the adsorbent particle—to evaluate the performance of each material for a mixture of 0.15 bar CO_2 and 0.75 bar N_2.[33]

Fig. 6a demonstrates the relatively poor performance of MOF-177 with CO_2 breakthrough occurring rapidly at 40 °C. On the other hand, $Mg_2(dobdc)$ has a significantly longer breakthrough time and outperforms zeolite NaX. Fig. 6c shows the quantity of CO_2 adsorbed at breakthrough, defined as when the outlet gas stream contains 1 mol % of CO_2. Importantly, $Mg_2(dobdc)$ exhibits longer breakthrough times and greater amounts of CO_2 adsorbed over the entire temperature range. Longer breakthrough times are desirable from a practical point of view because this implies a less frequent requirement for regeneration. Fig. 5b also shows the IAST calculations of wt % of CO_2 adsorbed from the same mixture as a function of temperature. The IAST results presented in Fig. 5b are slightly higher than the corresponding ones shown in Fig. 6c for the adsorber breakthrough simulations, because IAST allows the system to reach equilibrium over the entire bed. In the breakthrough calculations, the operation is terminated when the exit gas reaches the selected purity level of 1 mol % CO_2, implying that portions of the bed are not entirely in equilibrium with the inlet gas and are therefore underutilized.

Working capacity

The working capacity corresponds to the actual amount of CO_2 that can be captured during a full adsorption/desorption cycle and is thus a critically important parameter in evaluating the potential of any adsorbent in a real process. As such, working capacities were estimated for MOF-177, $Mg_2(dobdc)$, and zeolite NaX based on an idealized temperature swing adsorption system described previously by Berger and Bhown (see Fig. 1).[12] In this simplified model, flue gas at an initial temperature, T_0, with a composition of 0.15 bar CO_2, 0.75 bar N_2, and 0.1 bar of other minor components, enters a packed bed column containing the
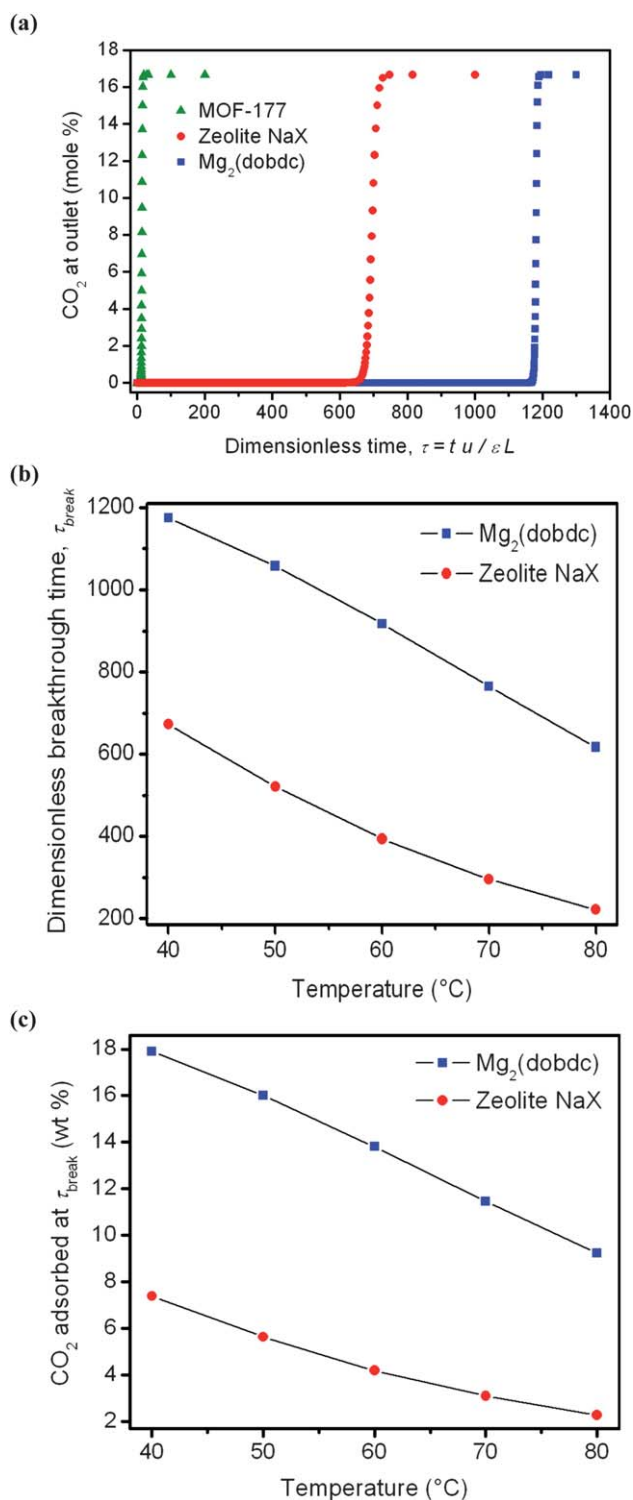
(a)

(b)

(c)

Fig. 6 (a) Simulated breakthrough curves for MOF-177, Mg$_2$(dobdc), and zeolite NaX at 40 °C for a gas mixture of 0.15 bar CO$_2$ and 0.75 bar N$_2$. The x-axis is a *dimensionless* time, t, obtained by dividing the actual time, t, by the contact time between the gas and the crystallites.[33] For a given adsorbent, under chosen operating conditions, the breakthrough characteristics are uniquely defined by t, allowing the results presented here to be equally applicable to laboratory scale equipment as well as to industrial scale adsorbers. (b) Simulated breakthrough time, t_{break}, as a function of temperature for Mg$_2$(dobdc) and zeolite NaX with a 0.15 bar CO$_2$ and 0.75 bar N$_2$ input gas mixture. The breakthrough time is

adsorbing material. As the flue gas travels through the bed, CO$_2$ is selectively adsorbed, and an N$_2$-rich stream exits from the end of the column. Once the percentage of CO$_2$ coming off of the column rises above a certain threshold value, regeneration is necessary. The incoming flue gas is redirected to another bed, while the saturated bed is heated to the desorption temperature, T_d. High-purity CO$_2$ is desorbed from the bed during heating, causing the pressure to increase and a CO$_2$-rich gas stream to be forced out the open end of the column. Once the bed has equilibrated at T_d, no more CO$_2$ will elute, and an N$_2$ purge is used to push the remaining CO$_2$ out of the column. This is continued until the CO$_2$ coming off the column falls below a desired purity level, at which point the column is cooled and readied for the next cycle. Such an adsorption cycle has already been validated experimentally using zeolites as a means of extracting high purity CO$_2$ from a CO$_2$/N$_2$ mixture.[34]

Based on this model, a working capacity can be approximated as the difference between the amount of CO$_2$ adsorbed at 0.15 bar and T_0 and the amount of CO$_2$ adsorbed at 1 bar and T_d, the latter of which corresponds to the amount of CO$_2$ that remains on the bed at the desorption temperature.[12] The CO$_2$ adsorption values used in these calculations were based on the pure component fits of the CO$_2$ isotherms. If anything, this model will over-estimate the actual working capacity for a material with low CO$_2$/N$_2$ selectivity, since the gas desorbed at T_d will be less than 100% CO$_2$. However, it should be reasonably accurate for any highly selective adsorbent and serves as a useful and easily calculated metric for comparing different materials.

The working capacities calculated for MOF-177, Mg$_2$(dobdc), and zeolite NaX assuming a flue gas temperature of $T_0 = 40$ °C are plotted in Fig. 7. Here, Mg$_2$(dobdc) reaches a positive working capacity at a regeneration temperature of $T_d = 90$ °C and attains a value of 4.85 mmol/g (17.6 wt %) at $T_d = 200$ °C. Furthermore, Mg$_2$(dobdc) outperforms zeolite NaX at all desorption temperatures, due primarily to its higher surface area and stronger adsorption sites. Significantly, MOF-177 does not exhibit a positive working capacity at any desorption temperature up to 200 °C. By analogy, other metal–organic frameworks possessing only weak physisorptive sites are not expected to be of utility for CO$_2$ capture *via* TSA. Note that, in all cases, the working capacity approaches a maximum value at high desorption temperatures, as the amount of CO$_2$ that remains adsorbed approaches zero. Consequently, there is a tradeoff between energy costs for heating the bed to higher temperatures and increased working capacities. The optimal desorption temperature for a given material, as well as the optimal CO$_2$ binding energy for a given set of power plant constraints, is dependent on many variables, and further studies considering the energetic implications and optimization of TSA CO$_2$ capture processes with strongly adsorbing metal–organic frameworks are currently underway.

While the absolute uptake of CO$_2$ is often used as a metric for comparing different materials, the working capacity is a far more important indicator of true performance. The working capacity in any TSA process is directly related to the temperature dependence of the CO$_2$ adsorption isotherms.[12] Determining the

0.15 bar CO$_2$ and 0.75 bar N$_2$ input gas mixture. The breakthrough time is defined as when the outlet gas stream contains 1 mol % CO$_2$. (c) The weight percent of CO$_2$ adsorbed at the breakthrough time as a function of temperature.

This journal is © The Royal Society of Chemistry 2011

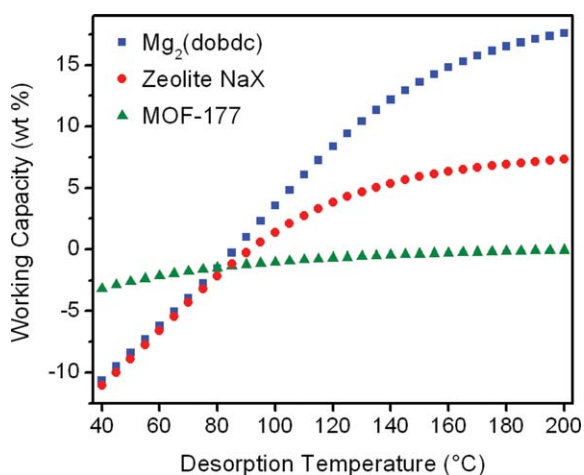*Energy Environ. Sci.*, 2011, **4**, 3030–3040 | **3037**

Fig. 7 Estimated working capacity as a function of desorption temperature, T_d, for MOF-177, Mg$_2$(dobdc), and zeolite NaX. The working capacity is calculated as the difference between the amount of CO_2 adsorbed at 0.15 bar at a flue gas temperature of 40 °C and the amount of CO_2 adsorbed at 1 bar at the desorption temperature. The pure component isotherm fits were used for performing the calculations.

working capacity for a solid adsorbent in a process with a temperature swing requires the measurement of high-temperature isotherms, which have been systematically collected for the first time in this work. Furthermore, the results reported here demonstrate that strong adsorption sites are necessary for a metal–organic framework to be useful in a TSA-based CO_2 capture process. Metal–organic frameworks that have high CO_2 uptake at 0.15 bar and flue gas temperatures, coupled with a rapid decrease in CO_2 adsorbed near atmospheric pressure and higher temperatures, will be most promising for CO_2 capture. In particular, high thermal stability of the metal–organic frameworks will be important so that the materials can withstand repeated cycling to the optimal desorption temperature.

Heat capacity

The regeneration step of a TSA process requires heating of the sorbent up to the desorption temperature, which, depending on the specific configuration of the power plant, may be as high as 200 °C. One parameter that is expected to impact considerably the efficiency of this process is the heat capacity (C_p) of the sorbent itself. The use of a low-heat capacity sorbent would be expected to afford a lower energy penalty for the regeneration step, which would be of significant benefit for reducing the total energy cost of post-combustion CO_2 capture.

The heat capacities for evacuated samples of MOF-177 and Mg$_2$(dobdc) recorded under a flow of N$_2$ are presented in Fig. 8. Interestingly, Mg$_2$(dobdc) initially exhibits a slight decrease in its heat capacity curve at temperatures up to 60 °C, presumably due to the desorption of bulk N$_2$ from the pores of the framework. Such an effect is not observed when the heat capacity measurement is conducted under a continuous He flow, since the adsorption of He is negligible across this temperature range (see Fig. S4†). In contrast, MOF-177, which adsorbs only a small quantity of N$_2$ at these temperatures, exhibits a nearly linear increase in the heat capacity with temperature. At temperatures
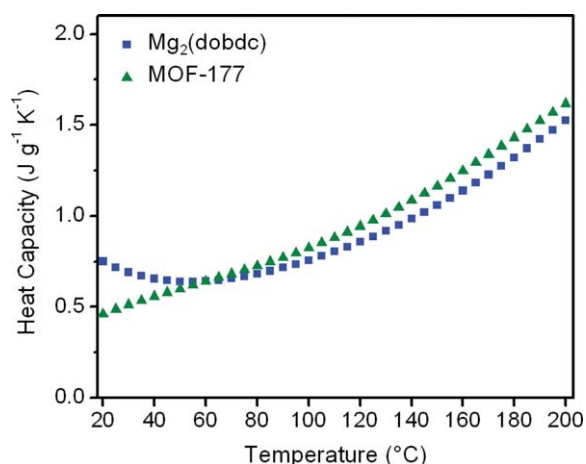

Fig. 8 Heat capacity of MOF-177 (green triangles) and Mg$_2$(dobdc) (blue squares) as a function of temperature measured under N$_2$.

above 60 °C, the heat capacities of the two materials are similar, reaching *ca.* 1.6 J g^{-1} K^{-1} at 200 °C. Nevertheless, consideration of the effect of adsorbed species on the heat capacity will be important in evaluating the regeneration energy requirements of any metal–organic framework in a TSA process since the material will contain significant amounts of adsorbed gas molecules (primarily CO_2) during the initial heating.

The heat capacity values reported here are comparable to the corresponding values for non-porous metal–organic frameworks and zeolites.[35] Importantly, the heat capacities are considerably lower than those of aqueous alkanolamine solutions, which carry a significant disadvantage in that the water in which the amine molecules are dissolved must also be heated to the desorption temperature of CO_2 (typically > 100 °C). For example, for a 30 wt % monoethanolamine (MEA) solution, the heat capacity at 25 °C is 3.73 J g^{-1} K^{-1}, which is close to the corresponding value for pure water (4.18 J g^{-1} K^{-1} at 25 °C), and is more than four times larger than the heat capacities of the metal–organic frameworks studied here.[36] Although the heat capacities of the metal–organic frameworks increase with temperature, the values at 200 °C are still less than half of the heat capacity of the MEA solution. This result highlights one of the key advantages of adopting a temperature swing adsorption process employing a metal–organic framework or other porous solid, wherein the contribution to the energy penalty arising from heating the adsorbent would be greatly reduced compared to the conventionally employed aqueous amine solutions.

Conclusions

The forgoing results demonstrate the importance of strong binding sites in metal–organic frameworks for post-combustion CO_2 capture using temperature swing adsorption. Frameworks with homogenous pore surfaces containing only weak adsorption sites are impractical for such a process, due to a poor selectivity and low working capacity. We have demonstrated that studying materials with strong CO_2 binding sites necessitates the use of a dual-site Langmuir adsorption model to adequately describe the adsorption profile, even when only the low-pressure range is to be considered for assessment of the material properties. Promising metal–organic frameworks are not limited to those with open metal sites. Work is

currently underway to evaluate frameworks with other pore surface functionalities for TSA CO_2 capture and to study the effect of minor flue gas components on the framework properties. Indeed, materials possessing functionalities such as amino groups, which also give rise to strong CO_2-adsorbent interactions, may be less likely to be poisoned by other flue gas components such as H_2O, NO_x, or SO_x. The synthesis of new materials that exhibit improved chemical robustness towards these impurities will also be a crucial endeavor in the development of next-generation CO_2 capture materials.

Acknowledgements

Notes and references

1 B. Metz, O. Davidson, H. de Coninck, M. Loos and L. Meyer, *Intergovernmental Panel on Climate Change. Special Report on Carbon Dioxide Capture and Storage*, Cambridge University Press, Cambridge, 2005., http://www.ipcc.ch/.

2 *CO₂ Emissions from Fuel Combustion*, International Energy Agency, Paris, 2010, http:/www.iea.org.

3 R. S. Haszeldine, *Science*, 2009, **325**, 1647.

4 S. M. Klara, R. D. Srivastava and H. G. McIlvried, *Energy Convers. Manage.*, 2003, **44**, 2699.

5 G. T. Rochelle, *Science*, 2009, **325**, 1652.

6 J. D. Figueroa, T. Fout, S. Plasynski, H. McIlvried and R. D. Srivastava, *Int. J. Greenhouse Gas Control*, 2008, **2**, 9.

7 (a) M. Eddaoudi, J. Kim, N. Rosi, D. Vodak, J. Wachter, M. O'Keeffe and O. M. Yaghi, *Science*, 2002, **295**, 469; (b) S. Kitagawa, R. Kitaura and S.-I. Noro, *Angew. Chem., Int. Ed.*, 2004, **43**, 2334; (c) R. Matsuda, R. Kitaura, S. Kitagawa, Y. Kubota, R. V. Belosludov, T. C. Kobayashi, H. Sakamoto, T. Chiba, M. Takata, Y. Kawazoe and Y. Mita, *Nature*, 2005, **436**, 238; (d) A. R. Millward and O. M. Yaghi, *J. Am. Chem. Soc.*, 2005, **127**, 17998; (e) H. Furukawa, M. A. Miller and O. M. Yaghi, *J. Mater. Chem.*, 2007, **17**, 3197; (f) G. Férey, *Chem. Soc. Rev.*, 2008, **37**, 191; (g) S. Ma, D. Sun, J. M. Simmons, C. D. Collier, D. Yuan and H. C. Zhou, *J. Am. Chem. Soc.*, 2008, **130**, 1012; (h) R. E. Morris and P. S. Wheatley, *Angew. Chem., Int. Ed.*, 2008, **47**, 4966; (i) P. L. Llewellyn, S. Bourrelly, C. Serre, A. Vimont, M. Daturi, L. Hamon, G. De Weireld, J.-S. Chang, D.-Y. Hong, Y. K. Hwang, S. H. Jhung and G. Férey, *Langmuir*, 2008, **24**, 7245; (j) L. J. Murray, M. Dincă and J. R. Long, *Chem. Soc. Rev.*, 2009, **38**, 1294–1314; (k) B. Chen, S. Xiang and G. Qian, *Acc. Chem. Res.*, 2010, **43**, 1115.

8 (a) G. R. Li, R. J. Kuppler and H. C. Zhou, *Chem. Soc. Rev.*, 2009, **38**, 1477; (b) A. Ö. Yazaydin, R. Q. Snurr, T. H. Park, K. Koh, J. Liu, M. D. LeVan, A. I. Benin, P. Jakubczak, M. Lanuza, D. B. Galloway, J. J. Low and R. R. Willis, *J. Am. Chem. Soc.*, 2009, **131**, 18198; (c) D. M. D'Alessandro, B. Smit and J. R. Long, *Angew. Chem., Int. Ed.*, 2010, **49**, 6058; (d) S. Keski, T. M. van Heest and D. S. Sholl, *ChemSusChem*, 2010, **3**, 879; (e) G. Férey, C. Serre, T. Devic, G. Maurin, H. Jobic, P. L. Llewellyn, G. De Weireld, A. Vimont, M. Daturi and J. S. Chang, *Chem. Soc. Rev.*, 2011, **40**, 550; (f) J. M. Simmons, H. Wu, W. Zhou and T. Yildirim, *Energy Environ. Sci.*, 2011, **4**, 2177.

9 (a) K. Z. House, C. F. Harvey, M. J. Aziz and D. P. Schrag, *Energy Environ. Sci.*, 2009, **2**, 193; (b) M. Ishibashi, H. Ota, N. Akutsu, S. Umeda, T. Motaki, J. Izumi, A. Yasutake, T. Kabata and T. Kageyama, *Energy Convers. Manage.*, 1996, **37**, 929.

10 V. Mulgundmath and H. Tezel, *Adsorption*, 2010, **16**, 587.

11 (a) F. Debatin, A. Thomas, A. Kelling, N. Hedin, Z. Bacsik, I. Senkovska, S. Kaskel, M. Junginger, H. Müller, U. Schilde, C. Jäger, A. Friedrich and H. J. Holdt, *Angew. Chem., Int. Ed.*, 2010, **49**, 1258; (b) P. Aprea, D. Caputo, N. Gargiulo, F. Iucolano and F. Pepe, *J. Chem. Eng. Data*, 2010, **55**, 3655.

12 A. H. Berger and A. S. Bhown, *Energy Proc.*, 2011, **4**, 562.

13 (a) H. K. Chae, D. Y. Siberio-Pérez, J. Kim, Y. Go, M. Eddaoudi, A. J. Matzger, M. O'Keefe and O. M. Yaghi, *Nature*, 2004, **427**, 523; (b) C. Zheng, D. Liu, Q. Yang, C. Zhong and J. Mi, *Ind. Eng. Chem. Res.*, 2009, **48**, 10479; (c) D. Saha, Z. Bao, F. Jia and S. Deng, *Environ. Sci. Technol.*, 2010, **44**, 1820.

14 (a) N. L. Rosi, J. Kim, M. Eddaoudi, B. Chen, M. O'Keeffe and O. M. Yaghi, *J. Am. Chem. Soc.*, 2005, **127**, 1504; (b) S. R. Caskey, A. G. Wong-Foy and A. J. Matzger, *J. Am. Chem. Soc.*, 2008, **130**, 10870; (c) D. Britt, H. Furukawa, B. Wang, T. G. Glover and O. M. Yaghi, *Proc. Natl. Acad. Sci. U. S. A.*, 2009, **106**, 20637; (d) P. D. C. Dietzel, V. Besikiotis and R. Blom, *J. Mater. Chem.*, 2009, **19**, 7362; (e) H. Wu, J. M. Simmons, G. Srinivas, W. Zhou and T. Yildirim, *J. Phys. Chem. Lett.*, 2010, **1**, 1946; (f) L. Valenzano, B. Civalleri, S. Chavan, G. T. Palomino, C. O. Areán and S. Bordiga, *J. Phys. Chem. C*, 2010, **114**, 11185; (g) K. Sumida, C. M. Brown, Z. R. Herm, S. Chavan, S. Bordiga and J. R. Long, *Chem. Commun.*, 2011, **47**, 1157; (h) Z. Bao, L. Yu, Q. Ren, X. Lu and S. Deng, *J. Colloid Interface Sci.*, 2011, **353**, 549.

15 (a) P. D. C. Dietzel, T. Morita, R. Blom and H. Fjellvag, *Angew. Chem., Int. Ed.*, 2005, **44**, 6354; (b) M. Dincă and J. R. Long, *J. Am. Chem. Soc.*, 2005, **127**, 9376; (c) A. Vimont, J.-M. Goupil, J.-C. Lavalley, M. Daturi, S. Surblé, C. Serre, F. Millange, G. Férey and N. Audebrand, *J. Am. Chem. Soc.*, 2006, **128**, 3218; (d) H. R. Moon, N. Kobayashi and P. M. Suh, *Inorg. Chem.*, 2006, **45**, 8672; (e) M. Dincă, A. Dailly, Y. Liu, C. M. Brown, D. A. Neumann and J. R. Long, *J. Am. Chem. Soc.*, 2006, **128**, 16876; (f) P. D. C. Dietzel, B. Panella, M. Hirscher, R. Blom and H. Fjellvag, *Chem. Commun.*, 2006, 959; (g) M. Dincă, W. S. Han, Y. Liu, A. Dailly, C. Brown and J. R. Long, *Angew. Chem., Int. Ed.*, 2007, **46**, 1419; (h) P. D. C. Dietzel, R. Blom and H. Fjellvag, *Eur. J. Inorg. Chem.*, 2008, 3624; (i) Y. Liu, H. Kabbour, C. M. Brown, A. D. Neumann and C. C. Ahn, *Langmuir*, 2008, **24**, 4772; (j) P. D. C. Dietzel, R. E. Johnsen, H. Fjellvag, S. Bordiga, E. Groppo, S. Chavan and R. Blom, *Chem. Commun.*, 2008, 5125; (k) W. Zhou, H. Wu and T. Yildirim, *J. Am. Chem. Soc.*, 2008, **130**, 15268; (l) K. Sumida, S. Horike, S. S. Kaye, Z. R. Herm, W. L. Queen, C. M. Brown, F. Grandjean, G. J. Long, A. Dailly and J. R. Long, *Chem. Sci.*, 2010, **1**, 184.

16 (a) E. Neofotistou, C. D. Malliakas and P. N. Trikalitis, *Chem.–Eur. J.*, 2009, **15**, 4523; (b) S. Couck, J. F. M. Denayer, G. V. Baron, T. Remy, J. Gascon and F. Kapteijn, *J. Am. Chem. Soc.*, 2009, **131**, 6326; (c) B. Arstad, H. Fjellvag, O. K. Kongshaug, O. Swang and R. Blom, *Adsorption*, 2008, **14**, 755.

17 (a) K. K. Tanabe, Z. Wang and S. M. Cohen, *J. Am. Chem. Soc.*, 2008, **130**, 8508; (b) Y. S. Bae, O. K. Farha, J. T. Hupp and R. Q. Snurr, *J. Mater. Chem.*, 2009, **19**, 2131; (c) A. Demessence, D. M. D'Alessandro, M. L. Foo and J. R. Long, *J. Am. Chem. Soc.*, 2009, **131**, 8784; (d) C. J. Doonan, W. Morris, H. Furukawa and O. M. Yaghi, *J. Am. Chem. Soc.*, 2009, **131**, 9492; (e) E. D. Bloch, D. Britt, C. J. Doonan, F. J. Uribe-Romo, H. Furukawa, J. R. Long and O. M. Yaghi, *J. Am. Chem. Soc.*, 2010, **132**, 14382.

18 E. Poirier and A. Dailly, *Nanotechnology*, 2009, **20**, 204006.

19 S. S. Kaye, A. Dailly, O. M. Yaghi and J. R. Long, *J. Am. Chem. Soc.*, 2007, **129**, 14176.

20 K. S. Walton and R. Q. Snurr, *J. Am. Chem. Soc.*, 2007, **129**, 8552.

21 D. G. Archer, *J. Phys. Chem. Ref. Data*, 1993, **22**, 1441.

22 Y.-S. Bae and C.-H. Lee, *Carbon*, 2005, **43**, 95.

23 (a) E. J. Granite and H. W. Pennline, *Ind. Eng. Chem. Res.*, 2002, **41**, 5470; (b) M. S. Jassim and G. T. Rochelle, *Ind. Eng. Chem. Res.*, 2006, **45**, 2465; (c) K. B. Lee and S. Sircar, *AIChE J.*, 2008, **54**, 2293.

24 Note that various definitions of weight percent, wt %, are found in the literature, presenting a challenge when directly comparing the performance of different materials. In this work, wt % is defined as:
$$wt\ \% = \frac{mass\ gas\ adsorbed}{mass\ adsorbent\ +\ mass\ gas\ adsorbed} \times 100\%.$$ The other commonly used definition, which neglects the mass of the adsorbed gas in the denominator, is more appropriately referred to as the weight ratio: $wt\ ratio = \frac{mass\ gas\ adsorbed}{mass\ adsorbent}$.

25 T. J. H. Vlugt, R. Krishna and B. Smit, *J. Phys. Chem. B*, 1999, **103**, 1102.

26 O. F. Mertens, *Surf. Sci.*, 2009, **603**, 1979.

27 Z. R. Herm, J. A. Swisher, B. Smit, R. Krishna and J. R. Long, *J. Am. Chem. Soc.*, 2011, **133**, 5664.

28 A. L. Myers and J. M. Prausnitz, *AIChE J.*, 1965, **11**, 121.

29 O. Talu, *Adv. Colloid Interface Sci.*, 1998, **76–77**, 227.

30 (*a*) R. Krishna, S. Calero and B. Smit, *Chem. Eng. J.*, 2002, **88**, 81; (*b*) R. Krishna and J. M. van Baten, *Chem. Eng. J.*, 2007, **133**, 121.

31 R. Krishna and J. M. van Baten, *Phys. Chem. Chem. Phys.*, 2011, **13**, 10593.

32 (*a*) Y. Belmabkhout, G. Pirngruber, E. Jolimaitre and A. Methivier, *Adsorption*, 2007, **13**, 341; (*b*) S. Cavenati, C. A. Grande and A. E. Rodrigues, *J. Chem. Eng. Data*, 2004, **49**, 1095.

33 R. Krishna and J. R. Long, *J. Phys. Chem. C*, 2011, **115**, DOI: 10.1021/jp202203c, in press.

34 J. Merel, M. Clausse and F. Meunier, *Ind. Eng. Chem. Res.*, 2008, **47**, 209.

35 (*a*) K. T. Chue, J. N. Kim, Y. J. Yoo, S. H. Cho and R. T. Yang, *Ind. Eng. Chem. Res.*, 1995, **34**, 591; (*b*) L. Qiu, V. Murashov and M. A. White, *Solid State Sci.*, 2000, **2**, 841; (*c*) L.-F. Song, C.-H. Jiang, J. Zhang, L.-X. Sun, F. Xu, Y.-Q. Tian, W.-S. You, Z. Cao, L. Zhang and D.-W. Yang, *J. Therm. Anal. Calorim.*, 2009, **101**, 365; (*d*) L.-F. Song, C.-H. Jiang, J. Zhang, L.-X. Sun, F. Xu, W.-S. You, Y. Zhao, Z.-H. Zhang, M.-H. Wang, Y. Sawada, Z. Cao and J.-L. Zeng, *J. Therm. Anal. Calorim.*, 2009, **100**, 679.

36 R. H. Wieland, J. C. Dingman and D. B. Cronin, *J. Chem. Eng. Data*, 1997, **42**, 1004.